View metadata, citation and similar papers at core.ac.uk
brought to you by CORE
provided by Cranfield CERES

La Société Savante de l'Aéronautique et de l'Espace

52nd 3AF International Conference on Applied Aerodynamics
27 – 29 March 2017, Lyon - France

FP38-AERO2017-knowles

CONTROLLING UNSTEADY CAVITY FLOWS USING INTERNAL STRUCTURES

K Knowles[(1)], D Bacci[(1)], A J Saddington[(1)], B Newby[(2)], N J Taylor[(2)]

(1) Aeromechanical Systems Group, Centre for Defence Engineering, Cranfield University Defence Academy of the United Kingdom, Shrivenham, SN6 8LA. UK
K.Knowles@cranfield.ac.uk
(2) MBDA UK Ltd, PO Box 5, Filton, Bristol, BS34 7QQ

ABSTRACT

We report experimental measurements and preliminary analysis on a series of geometric modifications to a rectangular cavity, aimed at alleviating the severity of the aeroacoustic environment. The cavity had a length-to-depth ratio of 5 and a width-to-depth ratio of 1, and featured a simplified representation of a generic missile on the centre line. The modifications consisted of full width and depth ribs or "collars" with a cutout for the missile. Collars could be fitted at various combinations of locations in the cavity and were either straight (i.e. perpendicular to the cavity centre line), leaned or yawed. The cavity flowfield was characterised by surface pressure measurements along the ceiling. Judging from the available measurements the presence of collars modified the mean pressure distribution, and appeared to reduce the acoustic tones and generally lower the broadband noise.

1. INTRODUCTION

The drive towards reducing signatures on modern combat aircraft has led to an increase in designs with internal stores carriage. This, however, introduces aerodynamic complexities when the weapons bay doors are opened: so-called "open", "transitional" or "closed" cavity flows (see Fig. 1). Accordingly, there is a large body of published research into cavity flows, e.g. [1-18]. Most of this work, however, has concentrated on the idealised case of smooth-walled rectangular cavities.

Some published work has looked at CFD predictions of realistic, highly detailed cavities, including many ribs, but has not isolated the effects of the ribs [13]. Furthermore, the ribs modelled in [13] represented structural components of the aircraft and were a relatively small fraction of the overall cavity cross-sectional dimensions. Our recent work, however, appeared to be the first in the open literature that sought to isolate the effects of a rib on a cavity flow [14]. We showed that a suitably-sized and -located rib could have a substantial and beneficial effect on the levels of unsteadiness in a transonic cavity flow. The present work aims at identifying an arrangement of extended internal ribs or "collars" that can control the pressure fluctuation levels in a transonic cavity. In both the present work and [14] the ribs are larger than those that would be seen as part of the aircraft structure.

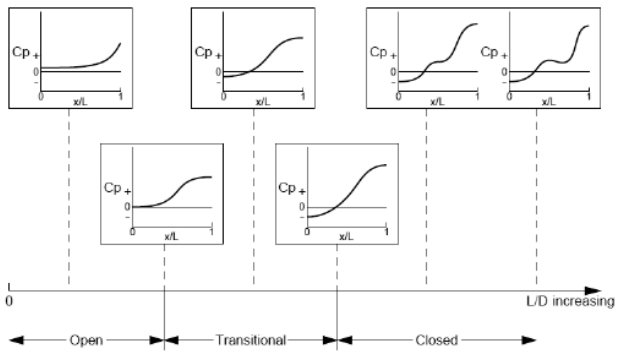

Figure 1. Characterisation of subsonic and transonic cavity flowfields (after [1])

2. EXPERIMENTATION

Experiments were conducted in Cranfield University's closed-circuit, ejector-driven transonic wind tunnel, located at the Defence Academy of the United Kingdom in Shrivenham (Fig. 2). This has a working section 206 mm high, 208 mm wide and 500 mm long. Compressed, dehumidified air is supplied from a Compair L110-10 compressor via a 34 m^3 storage tank to the tunnel's ejector system downstream of the working section. The test Mach number is set by a flexible nozzle upstream of the working section, a Boeing-flap diffuser system after the working section, and the ejector blowing pressure. For the present work the tunnel was set at a nominal freestream Mach number of 0.85 which, with a reservoir pressure of 800 kPa gives a tunnel run time of approximately 8 s. Actual freestream velocity was monitored via a Pitot-static probe mounted in the working section. Total pressure was measured on a Furness Controls FCO14 micromanometer, with a range of ±1000 mm water at an output voltage of ±5 V. The static pressure was measured with a Kulite 213-225 pressure transducer with a range of 0-1 bar (A). A K-type thermocouple measured the total freestream temperature.

Figure 2. Transonic wind tunnel with side door removed

Table 1. Typical run conditions

Quantity	Value	Δ_{Dev}	σ_{Dev}	Units
M_∞	0.86	0.0027	0.0013	-
q_∞	34.0	0.1660	0.0799	kPa
p_∞	63.2	0.5566	0.2872	kPa
T_∞	259.0	5.3056	2.3482	K

Typical flow conditions for this study are summarised in Tab. 1. Here the Δ_{Dev} and σ_{Dev} columns indicate respectively the absolute maximum and the r.m.s. deviations from the reference value encountered in all the runs executed. The maximum deviation was 2% (though usually much less), while the repeatability of the results (i.e. the maximum deviation between any given pair of runs performed) was below 1%, for pressure coefficient and OASPL, and less than 2% for the frequency spectra.

The side-door of the tunnel was modified to contain a cavity whose opening was flush with the tunnel sidewall. The present study used a rectangular cavity of length L = 160 mm, width W = 32 mm and depth D = 32 mm, giving a length-to-depth ratio (L/D) of 5 and width-to-depth ratio (W/D) of 1.

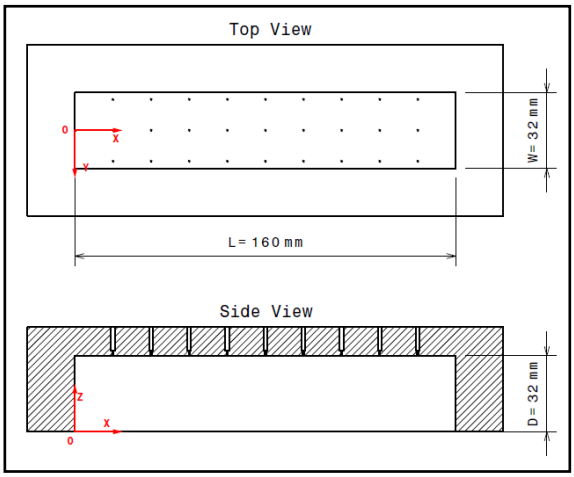

Figure 3. Cavity schematic showing tapping locations and co-ordinate system

The cavity ceiling was fitted with 27 static pressure tappings in 3 rows of 9 (Fig. 3). One row was on the cavity centreline, with the other two at ±81.25% of cavity semi-width. Each row had tappings equally spaced in the streamwise direction starting at x/L = 0.1 (where x is measured from the cavity leading edge). All data were sampled at a frequency of 10 kHz.

The pressure tappings were each connected via vinyl tubing of ~0.5 m length to a Scanivalve ZOC22B electronic pressure scanning module, containing 32 piezo resistive pressure sensors. The module maximum certified scan rate was 20 kHz, well within the current experiment requirements. For the current tests only one port per run could be monitored, so a full set of ceiling pressure data required a total of 27 wind tunnel runs. For each run 65 536 samples were used to calculate the time-averaged static pressure distribution and the frequency spectrum of the fluctuating pressure field. Data were also filtered, to remove aliasing effects, using a Bessel-type filter of 2nd order, with a cutting frequency of 3 kHz, a passband ripple of ±1.5dB at the cut frequency, and an attenuation slope of 40 dB per frequency decade. An experimentally-derived transfer function was applied to the measured pressures to compensate for the long pressure tubing.

Previous measurements of the boundary layer on the tunnel sidewall, just upstream of the cavity, showed a displacement thickness of 8 mm and a shape factor of 1.46 [18]. This profile is consistent with a turbulent boundary layer. It was estimated from these measurements that the boundary layer at the upstream lip of the current cavity was 8.8 mm thick.

A single, simplified representation of a generic missile (length-to-diameter ratio of 18, with a blunted tangent-ogive nose) was mounted centrally inside the cavity with up to 5 "collars" fitted around it at various streamwise locations. These collars spanned the full width and depth of the cavity with a cut-out to accommodate the missile (Fig 4).

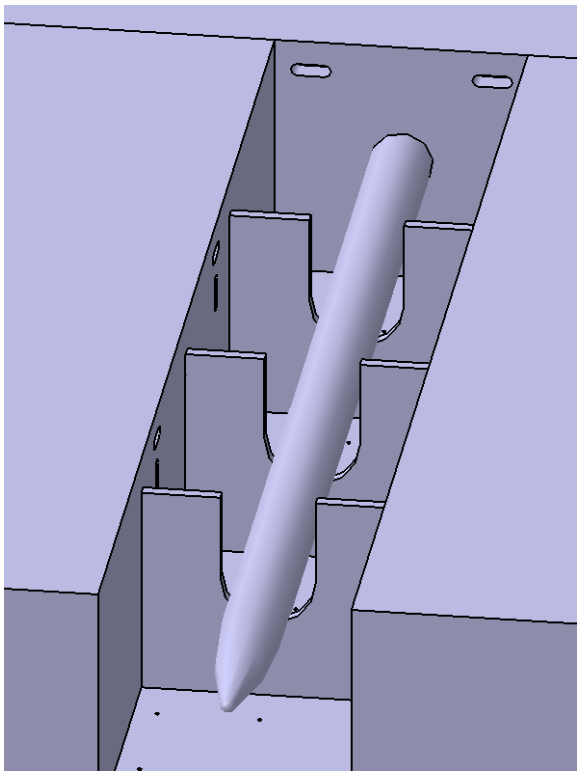

a)

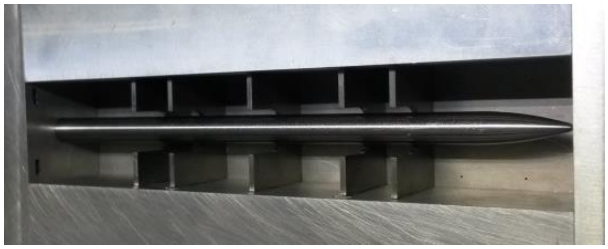

b)

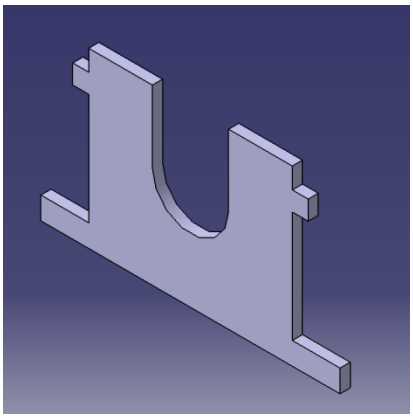

c)

Figure 4. Cavity, collars and missile model.
a) Assembled view of missile in cavity with 3 collars fitted (front wall of cavity removed for clarity).
b) Photograph of missile in cavity with 5 straight collars fitted.
c) Detail of a typical collar: the long and short tabs on each side are to locate the collar within slots in the cavity sidewalls.

Collars could be positioned at streamwise positions of 25%, 33%, 50%, 67% and 75% of cavity length and were located by vertical slots in the cavity sidewalls. Further collars were also tested that were "leaned" (or "pitched") forwards or backwards, or were yawed relative to the cavity and missile centrelines. The yawed and leaned collars were designed to fit into two of the existing locating slots. Thus, a leaned-back collar might have its lower locating tabs at x/L = 0.25 and its upper tabs at x/L = 0.33. An equivalent forward-leaned collar would have its upper tabs at x/L = 0.25 and its lower tabs at x/L = 0.33. Similarly, a yawed collar might be connected at x/L = 0.25 on one side and x/L = 0.33 on the other side. Such collars are described by these combinations of locating tab positions. In all cases the collars remained planar and extended to the same vertical height (the full depth of the cavity minus an allowance for the thickness of closed doors). Various combinations of yawed, leaned and straight collars were tested.

3. DATA ANALYSIS

Given a discrete finite time series in the form x_n with $n = 1,2,\dots N$, sampled at a time-step dt, the discrete Fourier transform is defined as in Eq. 1.

$$\hat{X}_k = \frac{1}{N} \cdot \sum_{j=1}^{N} x_j \cdot e^{-\frac{2\pi k j \cdot i}{N}} \qquad (1)$$

Following this, the one sided power spectral density (PSD) is defined as in Eq. 2.

$$PSD(k) = \frac{2}{F_s} \cdot \hat{X}_k \cdot \hat{X}_k^* \qquad k = 1,2 \ldots . \frac{N}{2} + 1 \tag{2}$$

The associated frequency vector is then defined as by Eq. 3.

$$f = \left(0,1,2 \ldots . \frac{N}{2}\right) \cdot \frac{F_s}{2 \cdot N} \tag{3}$$

The common practice for a long time series is to divide it into a defined number, M, of shorter overlapping elements, calculate the PSD for each segment, and then take the average. This is done to reduce the variance of the estimation, which is proportional to $1/M$. In this study, the analysed time series were divided into blocks with 50% overlap and with a number of samples equal to the ratio F_s/F_r. A Hanning window was then applied to each block to reduce leakage effects. Finally, the PSD of the original signal was calculated by averaging the PSD of each block.

In post-processing pressure signals, it is useful to define the Sound Pressure Levels (SPL) and the Overall Sound Pressure Level (OASPL) calculated using Eqs. (4) and (5). These quantities are all expressed in decibels.

$$SPL(f) = 10\, log_{10}\left(\frac{PSD_{p_f}(f) \cdot \Delta f_{ref}}{p^2_{reference}}\right) \tag{4}$$

$$OASPL = 20\, log_{10}\left(\frac{\sigma_p}{p_{reference}}\right) \tag{5}$$

Here $p_{reference}$ is the minimum audible pressure, equal to $2\text{x}10^{-5}$ Pa, which is defined as the threshold of human hearing, and Δf_{ref} is a reference frequency, set equal to 1Hz, which is just used to make the new quantity non-dimensional. (From Eq.(2) PSD units are, for pressure signals, Pa^2/Hz). σ_p is the root mean square of the fluctuating pressure.

Finally, for the analysis of pressure gradients on the cavity ceiling the mean pressure coefficient was defined by Eq. 6.

$$\overline{C_p} = \langle \frac{2}{\gamma \cdot M_\infty} \cdot \left[\frac{p}{p_\infty} - 1\right] \rangle \tag{6}$$

Here the overbar indicates that the quantity has been time-averaged.

For the estimation of the error on the mean quantities the approach derived in [19] was used. Given a measurement of N samples, the relative error of the calculated mean of a generic signal x with respect to the true value can be estimated using the following formula:

$$\epsilon = \frac{\mu_x^{Calculated}}{\mu_x^{True}} = z_{score} \cdot \frac{1}{\sqrt{N'}} \cdot \frac{\sigma_x^{Calculated}}{\mu_x^{Calculated}} \tag{7}$$

In this equation z_{score} indicates how many standard deviations are necessary for a Gaussian distribution, of mean zero and unity standard deviation, to obtain a desired confidence level. N' is the corrected number of samples. According to [20] the number of independent observations is fewer than N because, if the time series is auto-correlated, each observation is not separated from the information in other observations. Given a discrete finite time series in the form x_n with $n = 1,2, \ldots N$, the auto-correlation coefficient, at a time-lag k, is defined by Eq. 8, with c_k given by Eq. 9.

$$r_k = \frac{c_k}{c_{k=0}} \tag{8}$$

$$c_k = \frac{1}{N-1} \cdot \sum_{n=1}^{N-k} (x_n - \bar{x}) \cdot (x_{n+k} - \bar{x}) \tag{9}$$

It is then possible to define the corrected number of samples, N', as given by Eq. 10.

$$N' = N \cdot \frac{1 - r_1}{1 + r_1} \tag{10}$$

Here r_1 is the lag-1 auto-correlation coefficient. Using this technique for each run, the measured percent error on mean pressure values and Mach numbers was always below 0.5%. For the PSD error estimation the procedure described in [21] was used. For a given confidence level p, it is possible to define the relation given by Eq. 11.

$$\frac{PSD_{Calculated}}{PSD_{True}} \in [\chi_k^2(1-p), \chi_k^2(p)] \cdot \frac{1}{k} \tag{11}$$

Here p expresses the desired confidence level, while χ_k^2 is the chi-square probability density function of k degrees of freedom, a number that can be estimated using the Eq. 12.

$$k = 2B_eT \tag{12}$$

B_e is the bandwidth of the window used to calculate the Fourier spectrum while T is the temporal length of the signal. In these experiments, using F_r = 20 Hz, an

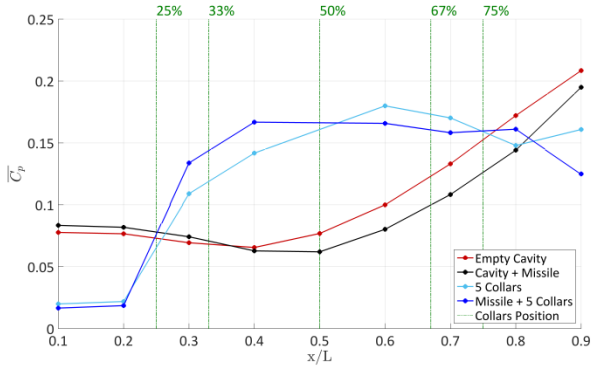

Figure 5. Streamwise distributions of mean C_p along cavity ceiling in various states: empty, clean cavity, no missile (red); cavity with missile, no collars (black); cavity with 5 collars, no missile (pale blue); and cavity with missile and 5 collars (dark blue). (Green lines indicate the five collar positions)

interval of confidence on PSD of -0.38 dB to +0.39 dB, relative to the calculated value, was obtained.

Finally, it is worth mentioning that for this study in all the above relations, a confidence level equal to 95% (or significance level equal to 0.05) was adopted.

4. RESULTS AND DISCUSSION

The pressure distribution measured in the clean cavity (red line in Fig. 5) was typical of an "open" flow (Fig. 1), with positive values of C_p throughout rising towards the rear wall. Judging from the available data the presence of the missile caused only a modest change to this distribution (black line in Fig. 5) – mostly a decrease in aft-cavity pressure. This contrasts with the findings of Ritchie [6], who investigated the effects of various store configurations on cavity flows and generally found an *increase* in cavity roof pressure in the presence of stores. Ritchie's cavity, however, was wider (*W/D* = 2.5 for *L/D* = 5) and his stores (one, two or three tangent-ogive cylinders) were mounted in the exit plane, rather than in a carriage position as here.

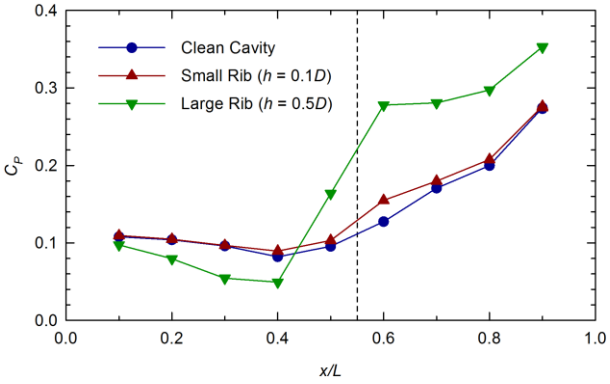

Figure 6. Centre-line C_p distributions along cavity ceiling from [14] (L/D = 5, W/D = 2.5, M = 0.85). (Dotted line represents location of rib)

Adding 5 straight collars (located at *x/L* = 0.25, 0.33, 0.5, 0.67, and 0.75 – see Fig. 4b) appears to cause a dramatic change to the mean pressure distributions (pale blue line in Fig 5). (Note that the tapping at *x/L* = 0.5 is obscured by the collar at that location.) "Upstream" of the first collar (i.e. at lower *x/L*) the mean pressure level appears depressed by comparison with the clean cavity, whereas "downstream" of the first collar pressure levels are raised. This effect on the mean C_p distribution appears consistent with the findings of [14] for a single, large, rib of full span and half depth in a wider cavity (Fig. 6). As explained in [14], it is possible that this behaviour can be understood, in part, by considering the mean flowfield inside a clean cavity. Fig. 7 shows the results of a CFD simulation for a similar narrow cavity, with mean streamlines visualised using line integral convolution (LIC) of the velocity field [12]. As shown in Fig. 7a, the main feature of the flowfield is a large recirculation in the centre of the cavity. The raised C_p values over much of the cavity suggest a slowing of this recirculating mean flow, with increased speeds near the upstream end causing the lowered pressure there.

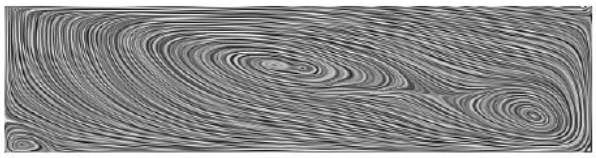

a) x-z plane at y/W = 0.5

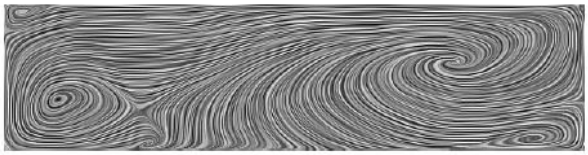

b) x-y plane at z/D = 0.5

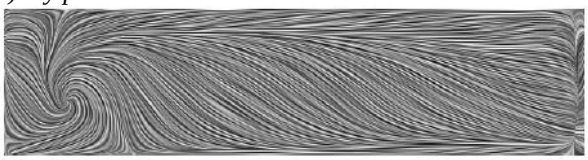

c) Cavity roof (x-y plane at z/D = 1)

e) Upstream wall

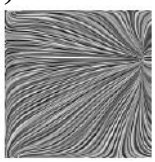

f) Downstream wall

Figure 7. LIC visualisation of CFD-predicted cavity flowfield (L/D = 4, W/D = 1, M = 0.8, freestream flow from left to right in a, b, c)[12]

One of the key features to note from the flow visualisation of Fig. 7 is that the mean flowfield in such

narrow cavities is notably asymmetric. This is in contrast to the flowfield in wider cavities (W/D > ~2) under similar conditions (M, L/D). Wider cavities of this length-to-depth ratio are generally seen to feature two symmetrically-arranged focus sinks at the upstream end of the cavity roof. The present work has not yet confirmed experimentally whether the asymmetric pattern shown in Fig. 7 exists in the current clean cavity, but it is reasonable to expect that this would be the case.

Measurements of unsteady pressures revealed typical open-flow-type spectra for the clean cavity and cavity with missile (Fig 8). The frequencies of the Rossiter modes [2], shown in Fig. 8, were calculated using the modified Rossiter equation proposed by Heller at al. [22] to account for temperature (and, therefore, speed of sound) variation within the cavity. Tones are seen at the first 3 Rossiter frequencies in both cases. The presence of the missile does not have a substantial effect on the acoustic spectrum. Ritchie found similar results when he placed missiles in the exit plane of a cavity [6].

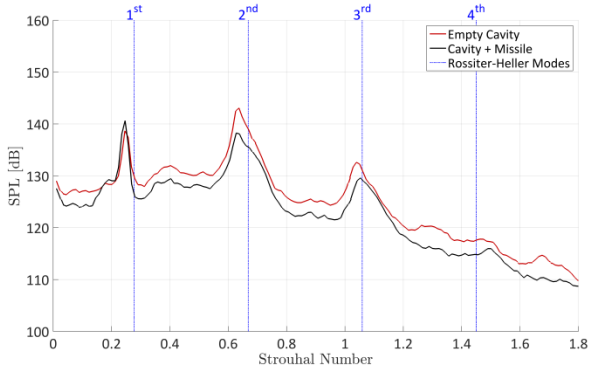

Figure 8. Unsteady pressure spectra on cavity ceiling at x/L = 0.9 for empty, clean cavity and cavity with missile (no collars)

Judging from the available data, many of the collar combinations appear to alleviate the flow unsteadiness and lower the magnitude of the first three Rossiter tones in the cavity. Fig. 9 presents some typical results. The clean cavity results (red line) are included for comparison. The collar combinations presented are: 5 straight collars as shown in Fig. 4b (yellow line); 3 collars, 1 leaned forward (from x/L = 33% to 25%) and 2 leaned back (from x/L = 50% to 67% and 67% to 75%) (black line); 4 collars, 2 of them straight ones at the front and 2 leaned back at the rear (green line); and 3 collars, 1 yawed at the front and 2 leaned back at the rear (blue line).

The 5 straight collars appeared to remove the first 3 Rossiter modes completely and generally lower the broadband level by around 5dB throughout the spectrum. This still left a tone, however, around the 4th Rossiter mode at a lower frequency than the uncontrolled case but at a higher level. This tone was effectively removed by using two straight collars in the front half of the cavity and two swept-back collars in the rear half.

It is noteworthy from Fig. 9 that the two configurations that feature forward-leaned or yawed collars in the front part of the cavity, both show a significant tone between the 3rd and 4th Rossiter modes. It is not yet clear why this is, but such configurations appear to be less beneficial than others examined here.

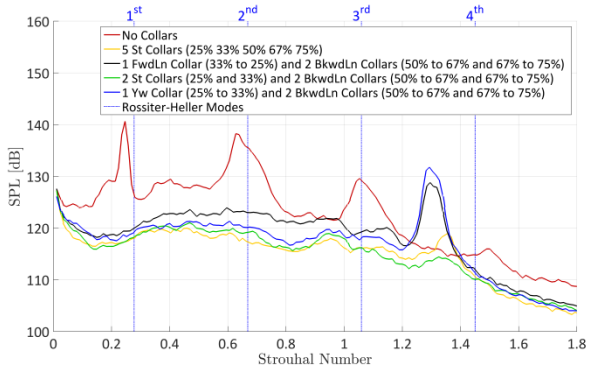

Figure 9. Unsteady pressure spectra on cavity ceiling at x/L = 0.9 for cavity with missile and various combinations of collars

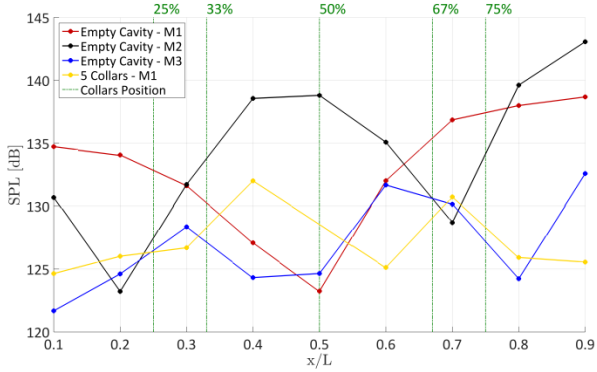

Figure 10. Mode shape comparison along the centreline of the ceiling for modes 1-3 of the empty cavity and mode 1 for the cavity with 5 straight collars. (Green lines indicate the five collar positions)

The above discussion was based on the spectra recorded near the aft wall of the cavity, at x/L = 0.9. In order to understand better the fluid-resonant behaviour occurring within the clean cavity and the impact of adding collars, the mode shapes for the first three tones have been determined by plotting the stream-wise variation in SPL (sound pressure level) associated with each tone in Fig. 10. The mode shapes obtained for the clean cavity's first (red line), second (black line) and

third (blue line) tones largely match the characteristic pattern observed by [23]. The first mode has a characteristic V shape; the second mode has a characteristic W shape; and the third mode nearly has the characteristic VW shape. It is not clear why the third mode does not exactly match the theoretical shape, but it may be a result of the experimental procedure, which required separate runs for each pressure tapping. Nevertheless, the overall observation supports the argument that resonant behaviour is occurring in the empty cavity because the mode shapes are characteristic of standing waves being formed along the length of the cavity.

With 5 straight collars fitted only a first Rossiter tone could be detected (and only towards the front of the cavity – nothing is seen in the plot at x/L = 0.9 in Fig. 9). Fig. 10 shows that this mode has amplitudes that are equivalent to the third mode of the empty cavity and 5-10 dB below the lowest amplitude of the first mode. Fig. 10 confirms that the 5-collars configuration has effectively removed the first Rossiter tone over the whole length of the cavity.

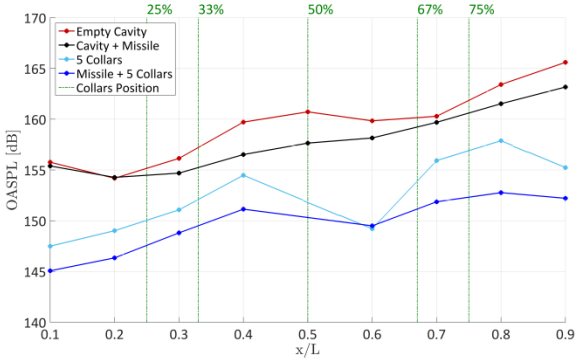

Figure 11. Overall sound pressure level distributions along the centreline of the ceiling of the empty cavity, cavity with missile, cavity with 5 straight collars and cavity with 5 straight collars and missile. (Green lines indicate the five collar positions)

The overall sound pressure level (OASPL) distribution along the cavity ceiling is plotted in Fig. 11 for the datum cases of clean cavity (red line) and cavity plus missile (black line), and for the equivalent cases with 5 collars (pale blue and dark blue lines). It can be seen that for the clean cavity the OASPL lies between 155 and 165 dB, rising towards the rear of the cavity. The addition of the missile has only a small effect on the OASPL distribution, lowering it slightly for the latter 2/3 of the cavity.

The addition of 5 straight collars appears substantially to reduce the OASPL over most of the cavity length, typically by 5 to 10 dB. When a missile is added to the cavity with 5 collars it generally lowers the measured OASPL levels by a further 2-5 dB throughout ther cavity, except for the measurement point at x/L = 0.6. In the final sub-bay of the cavity the presence of the missile appears particularly beneficial. OASPL computed for this case is consistently lower than 153 dB throughout the length of the cavity.

5. CONCLUSIONS

This paper has described an experimental investigation into alleviating cavity noise by using various configurations of "collars" inside the cavity. Collars appear to modify the mean pressure distribution in a manner that may partly be understood in the light of the clean cavity internal flow structure. Judging from the available data, the collars appear to suppress many or all of the cavity tones and generally reduce broadband noise levels. The noise suppression level may not be consistent throughout the cavity, however, and this needs further investigation.

This work has shown that simple modifications to a cavity internal geometry may significantly reduce noise levels. This approach has potential advantages over methods that involve external spoilers, deflectors or blowing [17] in that no actuation is required and there is no impact on airframe drag.

6. REFERENCES

1. Plentovich, E.B., Stallings, R.L., & Tracy, M.B. (1993). "Experimental Cavity Pressure Measurements at Subsonic and Transonic Speeds – Static Pressure Results". NASA Technical Report 3358.
2. Rossiter, J.E. (1964) "Wind-tunnel Experiments on the Flow over Rectangular Cavities at Subsonic and Transonic Speeds". Aeronautical Research Council report R&M 3438.
3. Heller, H.H. & Bliss, D.B. (1975). "Aerodynamically Induced Pressure Oscillations in Cavities - Physical Mechanisms and Suppression Concepts". Technical report AFFDL-TR-74-133.
4. Wilcox, F.L. (1990). "Experimental Measurements of Internal Store Separation Characteristics at Supersonic Speeds". RAeS Store Carriage, Integration and Release Conf, Bath, U.K. April.
5. Stallings, R.L., Plentovich, E.B., Tracy M.B. & Hemsch, M.J. (1995)." Measurements of Store Forces and Moments and Cavity Pressures for a Generic Store in and near a Box Cavity at Subsonic and Transonic Speeds". NASA Technical Memorandum 4611, Langley Research Center, VA, USA.
6. Ritchie, S.A. (2005). "Non-intrusive Measurements and Computations of Transonic

Cavity Flows with Applications to Aircraft Stores Release. PhD thesis, Cranfield University.
7. Geraldes, P. (2005). "Instabilities in Transonic Cavity Flows". PhD thesis, Cranfield University.
8. ESDU 02008 (2009): "Aerodynamics and Aero-acoustics of Rectangular Planform Cavities, Part I: Time-averaged Flow". Aerodynamics Committee, IHS Group ESDU International. May.
9. ESDU 04023b (2009): "Aerodynamics and Aero-acoustics of Rectangular Planform Cavities, Part II: Unsteady Flow and Aero-acoustics". Aerodynamics Committee, IHS Group ESDU International. May.
10. Atvars, K., Knowles, K., Ritchie, S. A., & Lawson, N. J. (2009). "Experimental and Computational Investigation of an 'Open' Transonic Cavity Flow". Proc. IMechE, Part G: Journal of Aerospace Engineering, 23(4), 357–368.
11. Lawson, S.J. & Barakos, G. (2010). "Review of Numerical Simulations for High-speed, Turbulent Cavity Flows". Progress in Aerospace Sciences, 47(3), 186-216.
12. Khanal, B. (2010). "A Numerical Investigation of the Aerodynamic Noise Generation Mechanism in Transonic Cavity Flows". PhD thesis, Cranfield University.
13. Morton, M.H., Cox, J.T. & Powell, E.A. (2012). "Initial Assessment of a CFD Application for Predicting Jet Fighter Aircraft Cavity Bay Acoustics for Subsonic and Supersonic Aircraft States". AIAA paper 2012-1624. DOI: 10.251416.2012-1624. April.
14. Knowles, K., Finnis, M.V. & Sapsford, L.D. (2015). "Effects of Internal Structures on Unsteady Cavity Flows", in *50th 3AF International Conference on Applied Aerodynamics*, 30 March - 01 April. Toulouse, France. 3AF. Paper no FP23-2015
15. Thangamani, V. (2013). "The Effects of Scaling on High Subsonic Cavity Flow and Control". PhD thesis, Cranfield University.
16. Thangamani, V., Knowles, K. & Saddington, A.J. (2014). "Effects of Scaling on High Subsonic Cavity Flow Oscillations and Control". *Journal of Aircraft* 51(2), 424-433. [DOI:10.2514/1.C032032]
17. Saddington, A.J., Thangamani, V. & Knowles, K. (2016). "Comparison of Passive Flow Control Methods for a Cavity in Transonic Flow", *Journal of Aircraft*, 2016, **53** (5), 1439-1447. [DOI: http://arc.aiaa.org/doi/abs/10.2514/1.C033365]
18. Thangamani, V. (2013). "The Effects of Scaling on High Subsonic Cavity Flow and Control". PhD thesis, Cranfield University.
19. Bruun, H. H. (1996). *Hot-Wire Anemometry Principles and Signal Analysis.* Oxford University Press, Oxford, UK.
20. Dawdy, D. R., & Matalas, N. C. (1964). *Statistical and Probability Analysis of Hydrologic Data, Part III: Analysis of Variance, Covariance and Time Series.* McGraw-Hill Book Company New York, USA.
21. Newland, D. E. (1993). *An Introduction to Random Vibrations, Spectral & Wavelet Analysis.* Longman Group Limited, Harlow, Essex, UK.
22. Heller, H.H., Holmes, D.G. and Covert, E.E., "Flow Induced Pressure Oscillations in Shallow Cavities", *Journal of Sound and Vibration*, 18 (4) pp 545-553, 1971
23. Tracy, M.B. and Plentovitch, E.B., "Characterization of Cavity Flow Fields Using Pressure Data Obtained in the Langley 0.3-meter Transonic Cryogenic Tunnel". NASA Technical Memorandum 4436, Langley Research Center, VA. 1993.